Elemental Mapping by Dawn Reveals Exogenic H in Vesta's Regolith

Thomas H. Prettyman,[1] David W. Mittlefehldt,[2] Naoyuki Yamashita,[1] David J. Lawrence,[3] Andrew W. Beck,[4] William C. Feldman,[1] Timothy J. McCoy,[4] Harry Y. McSween,[5] Michael J. Toplis,[6] Timothy N. Titus,[7] Pasquale Tricarico,[1] Robert C. Reedy,[1] John S. Hendricks,[8] Olivier Forni,[6] Lucille Le Corre,[9] Jian-Yang Li,[1] Hugau Mizzon,[6] Vishnu Reddy,[9,10] Carol A. Raymond,[11] Christopher T. Russell[12]

Using Dawn's Gamma Ray and Neutron Detector, we tested models of Vesta's evolution based on studies of howardite, eucrite, and diogenite (HED) meteorites. Global Fe/O and Fe/Si ratios are consistent with HED compositions. Neutron measurements confirm that a thick, diogenitic lower crust is exposed in the Rheasilvia basin, which is consistent with global magmatic differentiation. Vesta's regolith contains substantial amounts of hydrogen. The highest hydrogen concentrations coincide with older, low-albedo regions near the equator, where water ice is unstable. The young, Rheasilvia basin contains the lowest concentrations. These observations are consistent with gradual accumulation of hydrogen by infall of carbonaceous chondrites—observed as clasts in some howardites—and subsequent removal or burial of this material by large impacts.

Spectra of asteroid 4 Vesta are characterized by strong absorption bands of FeO-bearing pyroxenes that are indistinguishable from spectra of howardite, eucrite, and diogenite (HED) meteorites (*1*). Identification of a family of small Vesta-like asteroids (vestoids) derived from Vesta has led to the consensus that Vesta is the HED parent asteroid (*2*). Studies of HEDs indicate that Vesta is differentiated (*3*–*6*). The canonical model for the petrologic evolution of Vesta based on HEDs indicates that Vesta was substantially melted within a very few million years of the solar system's formation, forming a molten core overlain by a shell of partially or totally molten silicates (*3*, *5*, *6*). Crystallization of a global silicate magma ocean produced an olivine-dominated mantle, a lower crust rich in low-Ca pyroxene ± olivine (diogenite), and an upper crust of mafic flows and intrusions (eucrite) (*3*, *5*, *6*). Alternatively, serial magmatism could have emplaced diogenite plutons within the lower crust or at the crust-mantle boundary (*5*). Impact excavation and mixing produced a polymict regolith with a varying diogenite-to-eucrite ratio, which produces howardites when lithified by impact (*3*, *5*–*7*). Modeling of regolith formation on 100- to 300-km-diameter asteroids shows the howarditic debris layer should be hundreds of meters thick (*8*).

Dawn's Gamma Ray and Neutron Detector (GRaND) is used to measure gamma rays and neutrons produced by cosmogenic nuclear reactions and radioactive decay to depths of a few decimeters within Vesta's surface (*9*). Concentrations and detection limits for several elements and constraints on elemental abundances, including effective atomic mass and neutron absorption, can be determined. With these measurements, GRaND allows us to distinguish between the whole-rock compositions of HED end-members (*10*) and other lithologies that may be present (*9*). Gamma ray and neutron mapping data were acquired over almost 5 months in a circular, polar low-altitude mapping orbit (LAMO) with an average altitude of 210 km (*11*, *12*). Here, we compare these direct measurements of the elemental composition of Vesta's regolith with HED meteorites.

The gamma-ray spectra acquired by the bismuth-germanate (BGO) scintillator enables the determination of global Fe/O and Si/O mass ratios (*12*). Our conservative estimate for Fe/O is 0.30 ± 0.04 and that for Si/O is 0.56 ± 0.06, giving an Fe/Si ratio of 0.54 ± 0.09. The different achondrite, chondrite, and stony iron meteorite groups have wide ranges in Fe/O and Fe/Si, with the aubrites, all chondrites, and mesosiderites being quite distinct from HEDs (Fig. 1A). Some angrites, ureilites, and the anomalous aubrite, Shallowater, overlap HED compositions on this plot (Fig. 1B), but their visible and infrared spectra are easily distinguishable from those of HEDs (*13*–*15*). Some ungrouped basaltic achondrites also fall within the field of HEDs. Mineralogically and compositionally, these are very similar to basaltic eucrites and would be difficult to distinguish from the latter with Dawn instrumentation (*16*). None of the ungrouped basaltic achondrites are regolith breccias. Thus, the characteristics of the debris layers on their parent asteroids are unknown.

[1]Planetary Science Institute, 1700 East Fort Lowell, Suite 106, Tucson, AZ 85719–2395, USA. [2]NASA Johnson Space Center, Houston, TX 77058, USA. [3]Johns Hopkins University Applied Physics Laboratory, Laurel, MD 20723, USA. [4]Smithsonian Institution, Washington, DC 20560–0119, USA. [5]Department of Earth and Planetary Sciences, University of Tennessee, Knoxville, TN 37996–1410, USA. [6]Institut de Recherche en Astrophysique et Planétologie, CNRS-Université de Toulouse, France. [7]U.S. Geological Survey Astrogeology Science Center, Flagstaff, AZ 86001, USA. [8]TechSource, Los Alamos, NM 87544, USA. [9]Max Planck Institute for Solar System Research, Katlenburg-Lindau 37191, Germany. [10]Department of Space Studies, University of North Dakota, Grand Forks, ND 96712, USA. [11]Jet Propulsion Laboratory, California Institute of Technology, Pasadena, CA 91109, USA. [12]Department of Earth and Space Sciences, University of California, Los Angeles, CA 90095, USA.

*To whom correspondence should be addressed. E-mail: prettyman@psi.edu

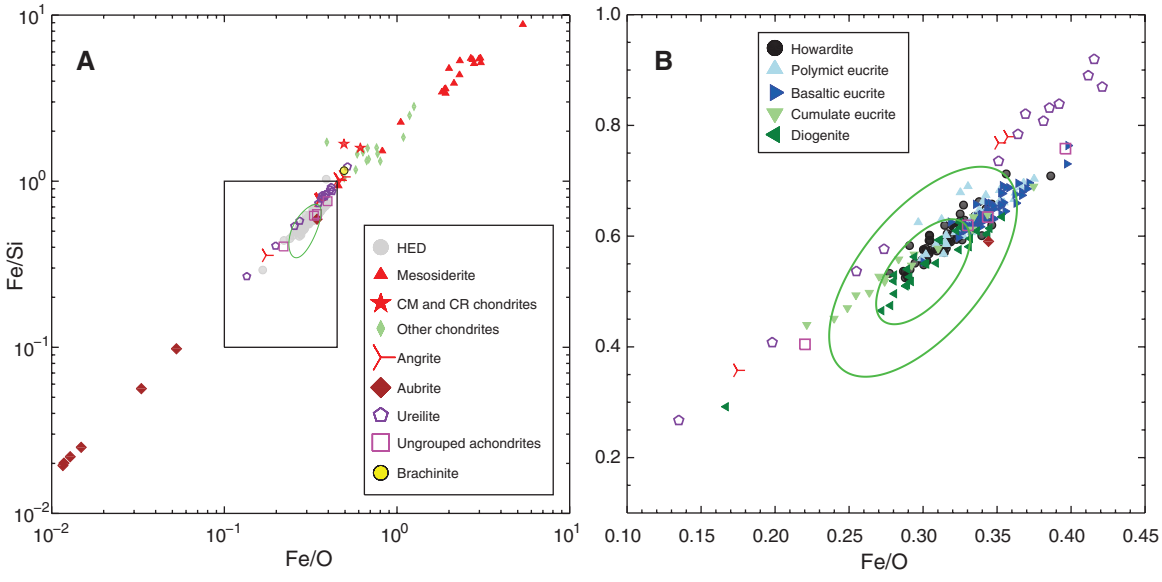

Fig. 1. Plots of Fe/Si versus Fe/O (by mass) for various achondrites, chondrites, and the stony iron mesosiderites are compared with HED meteorites. Box in (**A**) shows region expanded in (**B**). Error ellipses (1σ and 2σ) of the GRaND data are shown.

The GRaND error ellipse for the Fe/O and Fe/Si ratios includes howardites (Fig. 1B) but is skewed toward greater proportions of diogenite and cumulate eucrite (lower crustal materials) than basaltic eucrite. The Rheasilvia impact excavated and globally distributed lower crustal materials (*17*, *18*) and formed the family of vestoids (*19*). Howardites are likely derived from the vestoids, and thus represent Vesta's more basaltic-rich regolith before deposition of lower crustal materials ejected by the large, Rheasilvia impact. Nevertheless, the near equivalence in GRaND compositional data and howardites (Fig. 1) strengthens the Vesta-HED link and indicates that the vestan surface is consistent with eucrite and diogenite mixtures (*12*).

GRaND is sensitive to neutrons with kinetic energies within three ranges: fast (>0.7 MeV); epithermal (0.1 eV to 0.7 MeV); and thermal (<0.1 eV) (*9*, *12*). Neutron counting rates presented here were measured with a lithium-loaded glass (LiG) scintillator, which is sensitive to a mixture of thermal and epithermal neutrons (TPEs), and a boron-loaded plastic (BLP) scintillator, which separately measures epithermal and fast neutrons (*12*). Epithermal neutrons were also measured with a BLP-BGO coincidence signature (*12*).

Epithermal neutron counting rates (BLP_e), corrected for solid angle and variations in cosmic ray flux, depend on the abundance of H in Vesta's regolith and are relatively insensitive to other variations in composition for HED-like materials (*9*, *20*). For a homogeneous regolith, the abundance of H (micrograms per gram) is given by

$$[H] = k[C_0/C - 1] \quad (1)$$

where k = 2100, C is the corrected epithermal neutron counting rate, and C_0 is the counting rate for H-free materials (*12*, *20*). Zonally averaged neutron counting rates (Fig. 2) are systematically higher in the southern hemisphere. Assuming the highest counting rate corresponds to [H] = 0 μg/g, the 12% variation in epithermal counting rate implies a maximum zonally averaged [H] of 250 μg/g near the equator. Similarly, if H was the only compositional parameter then the variations in thermal plus epithermal (TPE) and (BLP_f) fast neutron counting rates would imply a maximum of 470 μg/g H (k = 8400) and 840 μg/g H (k = 11200), respectively.

These divergent estimates of [H] show that variations in the abundance of other elements affect the TPE and fast neutron measurements, which is not surprising given the variability of counting rates expected for H-free, whole-rock HED meteorite compositions (comparisons provided in Fig. 2). In contrast, the full-range variation of epithermal neutron counting rates (12%) is much larger than expected from HEDs (4%) and similar to that observed on the Moon by Lunar Prospector (11%) (*20*). Lunar [H] varies from about 50 μg/g from solar wind–implanted protons at equatorial latitudes to hundreds of micrograms per gram in permanently shadowed craters near the poles, which are thought to contain >1% g/g water ice (*20*, *21*).

Corrected BLP_e and TPE neutron counting rates mapped on 15° quasi-equal-area pixels show that the highest counting rates are contained within and centered on the Rheasilvia basin (Fig. 3). This observation is broadly consistent with instrument spatial-mixing of a compositionally uniform basin with surrounding regions. The lowest counting rates are at equatorial latitudes from about 60E to 225E. The high degree of correlation between the BLP_e and TPE neutron counting rates suggest that both are strongly influenced by variations in [H].

A scatter plot of the BLP_e and TPE neutron counting rates separates contributions from H and other elements (Fig. 4). The BLP_e neutron counting rate is relatively insensitive to changes in H-free composition, whereas the TPE neutron counting rate is strongly sensitive to variations in the absorption of neutrons by the regolith. For HEDs, variations in neutron absorption are caused

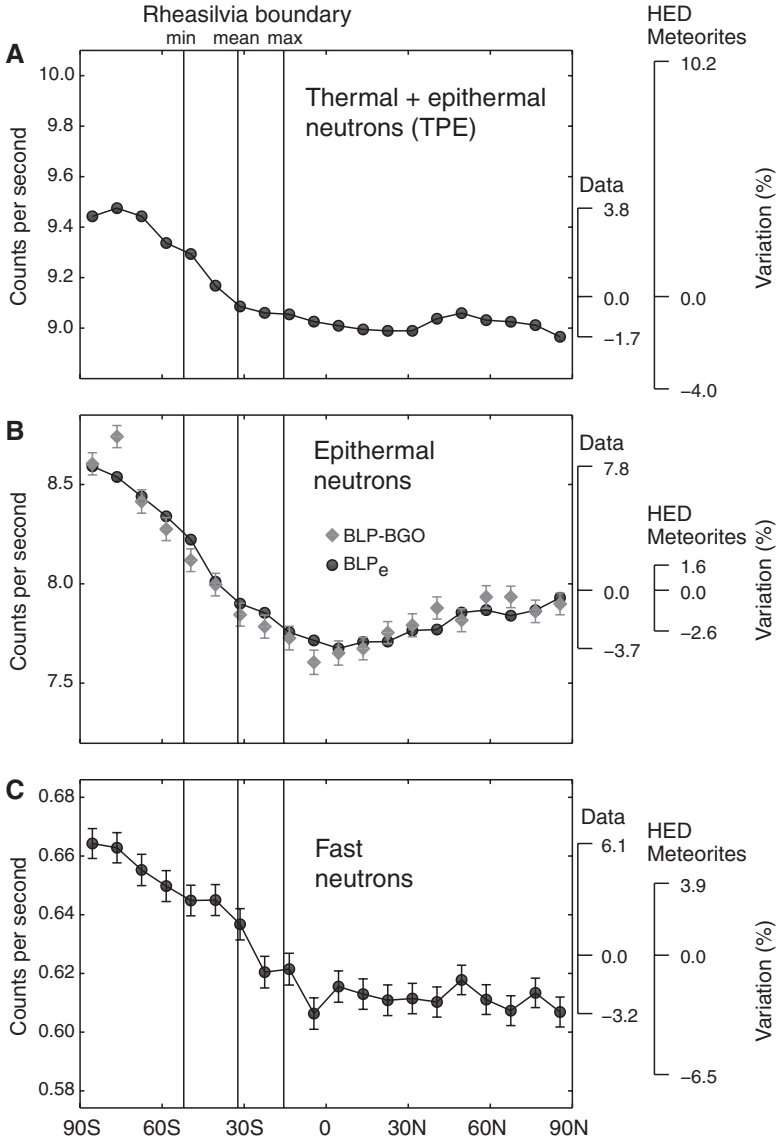

Fig. 2. Corrected neutron counting rates, binned by latitude vary with surface elemental composition. (**A**) Neutrons in the thermal + epithermal range (TPE) are sensitive to [H] and thermal neutron absorption (for example, by Fe). (**B**) Neutrons in the epithermal range are primarily sensitive to variations in [H]. Independent measurements of the epithermal neutrons, BLP_e and BLP-BGO (*9*, *12*), are shown. (**C**) Fast neutron measurements (BLP_f) are sensitive to variations in [H] and the average atomic mass of the regolith. All counting rates are elevated in the southern hemisphere, which contains the Rheasilvia impact basin (minimum, maximum, and mean latitudes for the basin are shown). In (A) to (C), the full-range variation in the counting data are compared with the range expected for HED meteorites, determined by modeling the response of GRaND to vestan neutrons for representative, H-free, whole-rock HED compositions (*10*, *12*). Average uncertainties for zonal TPE and BLP_e counting rates are 0.14 and 0.20%, respectively.

primarily by changes in the abundance of Fe, Ca, Al, Ti, and Mg (*9*). In the absence of H, diogenites, with relatively low Fe, Ca, and Al abundances, produce higher TPE neutron counting rates than that of basaltic eucrites, which have higher abundances of these elements.

For any H-free composition, increasing [H] causes the TPE and BLP_e counting rates to decrease in a predictable way (Fig. 4, red trend lines). GRaND data do not follow a single H trend line, indicating that neutron absorption is not uniform on Vesta's surface. Points within the Rheasilvia basin cluster to the right of the howardite trend line in Fig. 4, toward cumulate eucrites and diogenites. This is consistent with measurements of pyroxene band centers by Dawn's Visible-Infrared mapping spectrometer (VIR) (*22*), which show that Rheasilvia is more diogenitic than is the rest of Vesta. Hubble Space Telescope observations demonstrated the presence of the Rheasilvia basin, which was inferred to have excavated the lower crust or upper mantle (*23*); however, the multicolor camera data were interpreted to indicate high-Ca pyroxene and/or olivine and not the low-Ca pyroxene characteristic of diogenites detected with VIR.

Using Eq. 1 and assuming [H] = 0 μg/g for the maximum epithermal counting rate in Rheasilvia, the distribution of H on Vesta (Fig. 5) was determined from mapped epithermal neutron counting rates (Fig. 3A). This procedure gives a robust, lower bound on [H] at each map location, with uncertainties of ~50 μg/g. The global average [H] was 180 μg/g. Thus, Vesta's regolith contains at least 2.4×10^{11} kg of H within the 150 g/cm^2 depths sensed by GRaND. For a density like that of lunar soil, 1800 kg/m^3, Vesta's regolith would contain an average of 0.3 kg/m^3 of H in the approximately 80-cm-thick regolith layer sensed by GRaND. On the basis of comparison with data acquired with GRaND at Mars (*12*), the average [H] on Vesta could be higher: 800 μg/g. However, this estimate is very uncertain (±400 μg/g).

The map of [H] is compared with an albedo map in Fig. 5. The highest abundances of H correspond to the lowest-albedo regions. [H] and albedo are anticorrelated, with a linear Pearson correlation coefficient of –0.73 (*12*), suggesting that a dark, H-bearing component is mixed into the surface. Deviations from this correlation may arise from the large differences in the spatial resolution of the [H] and albedo maps and other sources of albedo variation, such as particle size or the presence of dark, H-free materials (such as impact melt or dewatered carbonaceous chondrites).

Hydrogen content is roughly associated with surface age, with the lowest [H] found in the younger Rheasilvia basin and the highest corresponding to dark, older units relatively uncontaminated with Rheasilvia ejecta (*17*, *24*). The young crater, Marcia (190E, 10N), a comparatively high-albedo feature within the dark equatorial region, is associated with a local minimum in [H] (Fig. 5). Another local minimum in [H] extending from Rheasilvia into the northwestern part of a basin containing Oppia is associated with relatively low crater density.

HED meteorite compositions show that Vesta accreted from volatile-poor materials and is similar to the Moon in its abundance of moderately volatile elements such as Na (*25*) and thus would have been very H-poor. Consequently, the H measured with GRaND does not have an endogenous source. Two exogenous sources are possible: implantation of solar wind H in regolith grains and the infall and survival of hydrous material from meteoroids.

Solar wind cannot explain the high-H contents (up to 400 μg/g) found in some areas. The lunar regolith contains far less H; 16 to 60 μg/g for soils and 11 to 116 μg/g for regolith breccias (*26*). Lunar soils contain 15 to 123 nmoles/g solar wind ^{20}Ne, and regolith breccias contain 56 to 335 nmoles/g (*12*). Kapoeta, a regolithic howardite (*7*), contains only 0.04 to 1.28 nmoles/g of ^{20}Ne in solar wind–dominated samples (*27*). Correcting the solar wind flux for heliocentric distance, the data show that Kapoeta had a shorter exposure than did lunar regolith breccias and cannot contain more than 100 μg/g solar wind H and likely much less (*12*).

The infall of carbonaceous chondritic material containing OH-bearing phyllosilicates is a viable alternative (*9*). A weak detection of an OH absorption feature in Earth-based infrared spectral measurements has been interpreted as arising from carbonaceous chondritic debris on Vesta (*28*), although this detection was not confirmed by other Earth-based observations (*29*). Admixture of carbonaceous chondritic material is one of two hypotheses advanced to explain lower-albedo regions seen in Dawn Framing Camera images (*30*).

Incorporation of hydrous carbonaceous chondritic debris in the regolith can quantitatively explain the measured concentrations of H and the association of H with low-albedo material. Chondritic clasts have been found in the HEDs, mostly in howardites (*12*). Most clasts are CM or CR chondrites; ~80% are CM (*31*). Modal abundances of clasts are typically 2 to 5% by volume, but an exceptional sample contains up to 60% clasts (*32*). Some clasts have been partially dehydrated during impact (*31*). The average H

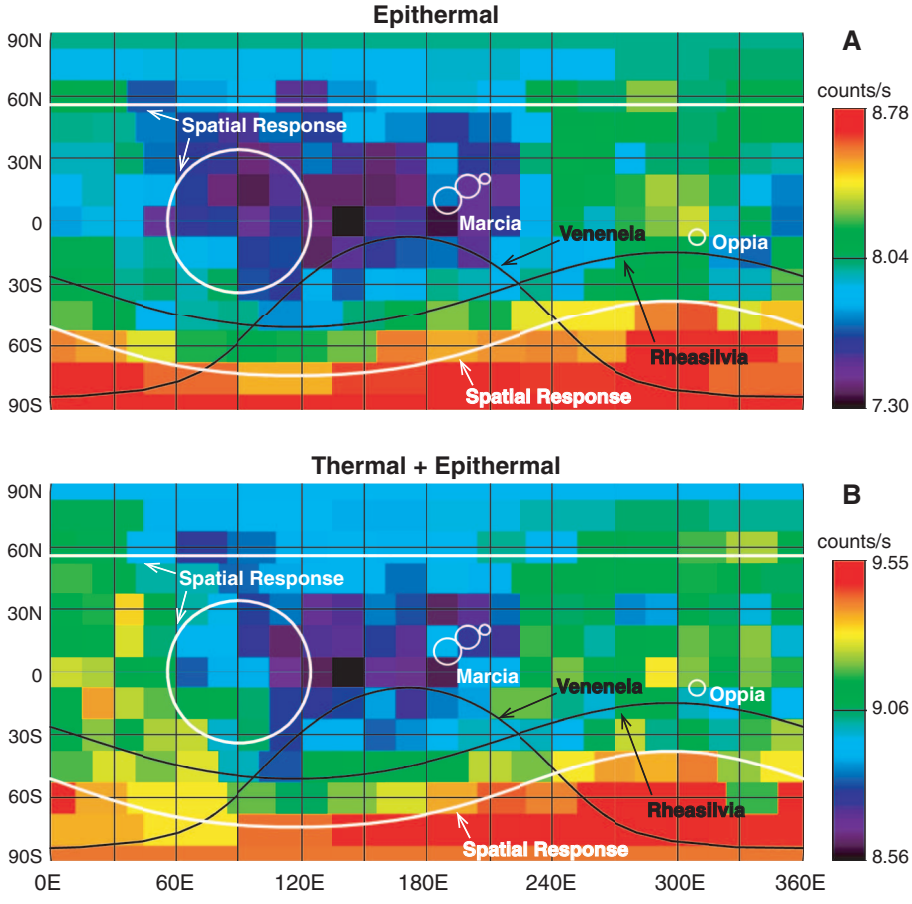

Fig. 3. Maps of corrected (**A**) epithermal (BLP_e) and (**B**) thermal + epithermal (TPE) neutron counting rates binned on 15° quasi-equal-area pixels reveal compositional variations on Vesta's surface. Longitude convention used is based on the Claudia system (*11*). The boundaries of two large-impact basins in the southern hemisphere are shown. Craters mentioned in the text are indicated. The spatial resolution (half-maximum) of GRaND is indicated as circles (white) for three subsatellite locations: the north pole, the equator, and at the center of Rheasilvia. Roughly half of the counts measured by GRaND at any location originate within the half-maximum. GRaND fully resolves features separated by a circle-diameter.

content of CM chondrites is 1.2 weight percent (*33*), and CR chondrites have comparable H contents (*34*). The abundances of carbonaceous chondrite clasts translate to 240 to 600 μg/g H for bulk howardites, assuming little dehydration has occurred, which is similar to abundances found on Vesta. Volatilization of hydrogen-bearing materials by high-velocity impacts may have resulted in the formation of pitted terrain (*35*); one

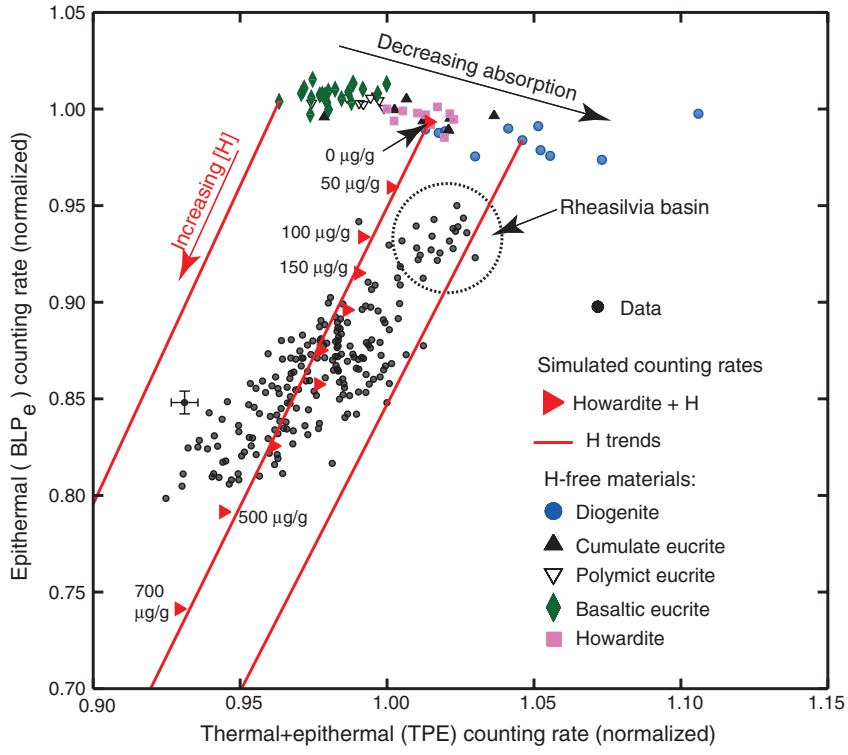

Fig. 4. Contributions from H and neutron absorption are distinguished by a scatterplot of the mapped epithermal (BLP_e) and thermal + epithermal (TPE) counting rates (Fig. 3). Representative error bars are shown. The data are compared with simulated neutron counting rates for HED whole-rock compositions (*12*). Counting rate trends with [H] are shown for selected compositions. [H] is indicated for selected points along the Howardite + H trend line. Both the models and data were arbitrarily normalized for this comparison.

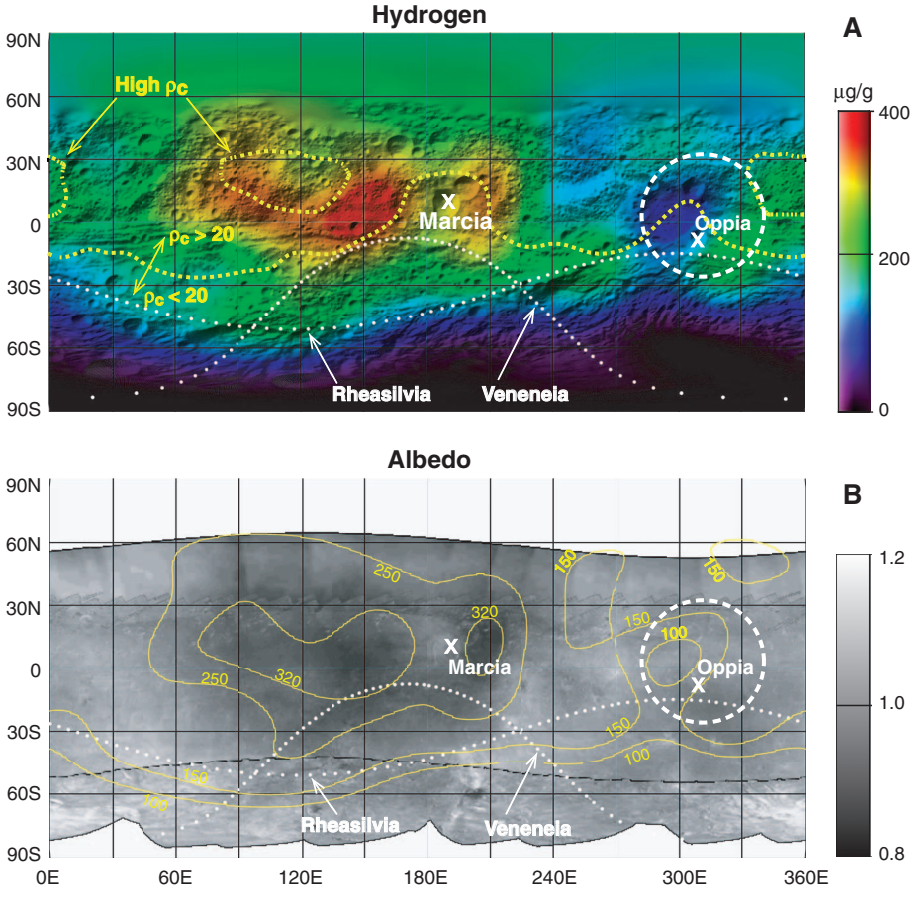

Fig. 5. A map of [H], superimposed on shaded relief (**A**), is compared with an albedo map (**B**) of Vesta (*12*, *30*, *37*). The dashed white line outlines a circular depression, containing crater Oppia (*24*). Approximate contours of smoothed crater density (ρ_C in craters per 10^4 km^2), superimposed in yellow on the [H] map indicate relative age of the surface (*24*). Yellow contours of [H], (in micrograms per gram), are superimposed on the map of albedo. Roughly 30% of Vesta's surface is contained within the 250 μg/g and higher contours.

such terrain corresponds to the low-[H] region around Marcia crater.

The extensive region on Vesta with elevated H content is not plausibly due to a localized enhancement in meteoroid flux or a single isolated impact—for example, fragments of the Veneneia basin impactor. Regolithic howardites such as Kapoeta contain CM, CR, and CI chondrite clasts (*31*) in modest abundance (*12*), which suggests accumulation over time from numerous impactors and asteroidal dust (*36*). Thus, the H-rich region of Vesta probably reflects a zone of more ancient regolith, on which the accumulation of chondritic debris has had a longer history. If Rheasilvia ejecta blanketed this region, it was much thinner than elsewhere on Vesta, so that subsequent gardening has mixed in more of the underlying ancient, carbonaceous chondrite-rich regolith.

The deposition of exogenic material is time-dependent, with H accumulating gradually on exposed surfaces. Accumulation is reset by impact excavation, volatilization, and mantling by ejecta. Thus, the [H] measured with GRaND provides a measure of the relative age of the vestan regolith on a global scale.

References and Notes

1. T. B. McCord, J. B. Adams, T. V. Johnson, *Science* **168**, 1445 (1970).
2. R. P. Binzel, S. Xu, *Science* **260**, 186 (1993).
3. D. W. Mittlefehldt, T. J. McCoy, C. A. Goodrich, A. Kracher, *Rev. Mineral. Geochem.* **36**, 4.1 (1998).
4. M. J. Drake, *Meteorit. Planet. Sci.* **36**, 501 (2001).
5. H. Y. McSween, D. W. Mittlefehldt, A. W. Beck, R. G. Mayne, T. J. McCoy, *Space Sci. Rev.* **163**, 141 (2011).
6. K. Keil, in *Asteroids III*, W. F. Bottke, A. Cellino, P. Paolicchi, R. P. Binzel, Eds. (Univ. Arizona Press in collaboration with the Lunar and Planetary Institute, Tucson, AZ, 2002), pp. 573–584.
7. P. H. Warren, G. W. Kallemeyn, H. Huber, F. Ulff-Møller, W. Choe, *Geochim. Cosmochim. Acta* **73**, 5918 (2009).
8. K. R. Housen, L. L. Wilkening, *Annu. Rev. Earth Planet. Sci.* **10**, 355 (1982).
9. T. H. Prettyman *et al.*, *Space Sci. Rev.* **163**, 371 (2011).
10. T. Usui, H. Y. McSween Jr., D. W. Mittlefehldt, T. H. Prettyman, *Meteorit. Planet. Sci.* **45**, 1170 (2010).
11. C. T. Russell *et al.*, *Science* **336**, 684 (2012).
12. Descriptions of data and methods are available as supplementary materials on *Science* Online.
13. T. H. Burbine, T. J. McCoy, J. L. Hinrichs, P. G. Lucey, *Meteorit. Planet. Sci.* **41**, 1139 (2006).
14. B. E. Clark *et al.*, *J. Geophys. Res.* **109**, (E2), E02001 (2004).
15. E. A. Cloutis *et al.*, *Meteorit. Planet. Sci.* **45**, 1668 (2010).
16. D. W. Mittlefehldt, *Meteorit. Planet. Sci.* **40**, 665 (2005).
17. P. Schenk *et al.*, *Science* **336**, 694 (2012).
18. R. Jaumann *et al.*, *Science* **336**, 687 (2012).
19. E. Asphaug, *Meteorit. Planet. Sci.* **32**, 965 (1997).
20. W. C. Feldman *et al.*, *J. Geophys. Res.* **106**, (E10), 23231 (2001).
21. A. Colaprete *et al.*, *Science* **330**, 463 (2010).
22. M. C. De Sanctis *et al.*, *Science* **336**, 697 (2012).
23. P. C. Thomas *et al.*, *Science* **277**, 1492 (1997).
24. S. Marchi *et al.*, *Science* **336**, 690 (2012).
25. D. W. Mittlefehldt, in *Treatise on Geochemistry*, D. H. Heinrich, K. T. Karl, Eds. (Pergamon, Oxford, 2007), pp. 291–324.
26. R. Bustin, E. K. Gibson Jr., in *The Second Conference on Lunar Bases and Space Activities of the 21st Century*, W. W. Mendell, Ed. (NASA, Washington, DC, 1992), pp. 437–445.
27. L. Schultz, L. Franke, *Meteorit. Planet. Sci.* **39**, 1889 (2004).
28. S. Hasegawa *et al.*, *Geophys. Res. Lett.* **30**, 2123 (2003).
29. A. Rivkin, L. McFadden, R. Binzel, M. Sykes, *Icarus* **180**, 464 (2006).
30. V. Reddy *et al.*, *Science* **336**, 700 (2012).
31. M. E. Zolensky, M. K. Weisberg, P. C. Buchanan, D. W. Mittlefehldt, *Meteorit. Planet. Sci.* **31**, 518 (1996).
32. J. S. Herrin, M. E. Zolensky, J. A. Cartwright, D. W. Mittlefehldt, D. K. Ross, *Proc. Lunar Planet. Sci. Conf.* **42**, 2806 (2011).
33. K. Lodders, B. J. Fegley, *The Planetary Scientist's Companion* (Oxford Univ. Press, New York, 1998).
34. J. F. Kerridge, *Geochim. Cosmochim. Acta* **49**, 1707 (1985).
35. B. Denevi, *Science* (2012).
36. M. Gounelle, M. E. Zolensky, J.-C. Liou, P. A. Bland, O. Alard, *Geochim. Cosmochim. Acta* **67**, 507 (2003).
37. J.-Y. Li *et al.*, *Icarus* **208**, 238 (2010).

Acknowledgments: We thank the Dawn team for spacecraft and instrument operations at Vesta. Portions of this work were performed by the Planetary Science Institute under contract with the Jet Propulsion Laboratory (JPL), California Institute of Technology; by JPL under contract with NASA; and by the NASA Dawn Participating Scientist Program. D. Bazell and P. Peplowski of Johns Hopkins University Applied Physics Laboratory assisted in fast-neutron data analysis. The Dawn mission is led by the University of California, Los Angeles, and managed by JPL under the auspices of the NASA Discovery Program Office. The Dawn data are archived with the NASA Planetary Data System.

Supplementary Materials

www.sciencemag.org/cgi/content/full/science.1225354/DC1
Supplementary Text
Figs. S1 to S27
Tables S1 to S4
References (*38*–*442*)

29 May 2012; accepted 13 August 2012
Published online 20 September 2012;
10.1126/science.1225354

Pitted Terrain on Vesta and Implications for the Presence of Volatiles

B. W. Denevi,[1]* D. T. Blewett,[1] D. L. Buczkowski,[1] F. Capaccioni,[2] M. T. Capria,[2] M. C. De Sanctis,[2] W. B. Garry,[3] R. W. Gaskell,[3] L. Le Corre,[4] J.-Y. Li,[3,5] S. Marchi,[6] T. J. McCoy,[7] A. Nathues,[4] D. P. O'Brien,[3] N. E. Petro,[8] C. M. Pieters,[9] F. Preusker,[10] C. A. Raymond,[11] V. Reddy,[4,12] C. T. Russell,[13] P. Schenk,[14] J. E. C. Scully,[13] J. M. Sunshine,[5] F. Tosi,[2] D. A. Williams,[15] D. Wyrick[16]

We investigated the origin of unusual pitted terrain on asteroid Vesta, revealed in images from the Dawn spacecraft. Pitted terrain is characterized by irregular rimless depressions found in and around several impact craters, with a distinct morphology not observed on other airless bodies. Similar terrain is associated with numerous martian craters, where pits are thought to form through degassing of volatile-bearing material heated by the impact. Pitted terrain on Vesta may have formed in a similar manner, which indicates that portions of the surface contain a relatively large volatile component. Exogenic materials, such as water-rich carbonaceous chondrites, may be the source of volatiles, suggesting that impactor materials are preserved locally in relatively high abundance on Vesta and that impactor composition has played an important role in shaping the asteroid's geology.

In July 2011, the Dawn spacecraft entered into orbit around Vesta, the second-most massive asteroid in the solar system. After initial Survey and High-Altitude orbits, Dawn spiraled down to its ~210-km Low-Altitude Mapping Orbit (LAMO) (*1*), allowing for acquisition of Framing Camera (FC) images (*2*) at pixel scales of <20 m, as well as high-resolution views of Vesta's geology. LAMO clear-filter images cover >70% of the surface (latitudes above ~55°N were in shadow). In this data set, we identified terrain with a distinct pitted morphology. Here, we describe this terrain and its implications for the presence and origin of volatiles on Vesta.

The most widespread occurrence of pitted terrain is associated with Marcia crater (~70-km diameter, Fig. 1A). Marcia is among the most recent large impacts on Vesta; using the methods of Marchi *et al.* (*3*), we estimate its age to be ~70 million years. Pitted terrain is found on otherwise smooth deposits located on the crater floor surrounding a small central peak, atop a slump terrace, and within portions of the continuous ejecta blanket. Pits lack raised rims, and on the floor they range in size from ~30 m (near the limit of resolution at 17 m per pixel) to just over 1 km in diameter (Fig. 1, B to D). Pits found in clusters on the slump terrace and ejecta blanket are smaller (largest sizes: ~250 m) and are often located where ejecta fills topographic lows (Fig. 1, A and F). On the floor, material that slumped down the crater walls appears to bury the pitted terrain in several areas; in others, pits may occur within the slump deposits (fig. S1). Toward the center of the floor where the deposit is probably thickest, pits increase in size, and their shapes become more

[1]The Johns Hopkins University Applied Physics Laboratory, Laurel, MD, USA. [2]Istituto di Astrofisica e Planetologia Spaziali, Istituto Nazionale di Astrofisica, Rome, Italy. [3]Planetary Science Institute, Tucson, AZ, USA. [4]Max Planck Institute for Solar System Research, Katlenburg-Lindau, Germany. [5]University of Maryland, College Park, MD, USA. [6]NASA Lunar Science Institute, Boulder, CO, USA. [7]National Museum of Natural History, Smithsonian Institution, Washington, DC, USA. [8]NASA Goddard Space Flight Center, Greenbelt, MD, USA. [9]Brown University, Providence, RI, USA. [10]Deutsches Zentrum fur Luft- und Raumfahrt (DLR), Institute of Planetary Research, Berlin, Germany. [11]Jet Propulsion Laboratory, California Institute of Technology, Pasadena, CA, USA. [12]University of North Dakota, Grand Forks, ND, USA. [13]University of California, Los Angeles, CA, USA. [14]Lunar and Planetary Institute, Houston, TX, USA. [15]Arizona State University, Tempe, AZ, USA. [16]Southwest Research Institute, San Antonio, TX, USA.

*To whom correspondence should be addressed. E-mail: brett.denevi@jhuapl.edu